

1.5D quasilinear model and its application on beams interacting with Alfvén eigenmodes in DIII-D

K. Ghantous,¹ N. N. Gorelenkov,¹ H. L. Berk,² W. W. Heidbrink,³ and M. A. Van Zeeland⁴

¹Princeton Plasma Physics Laboratory, PO Box 451, Princeton, New Jersey 08543-0451, USA

²Institute for Fusion Studies, University of Texas, 2100 San Jacinto Blvd., Austin, Texas 78712-1047, USA

³Department of Physics and Astronomy, University of California Irvine, Irvine, California 92697, USA

⁴General Atomics, PO Box 85608, San Diego, California 92186-560, USA

(Received 12 June 2012; accepted 20 August 2012; published online 26 September 2012)

We propose a model, denoted here by 1.5D, to study energetic particle (EP) interaction with toroidal Alfvénic eigenmodes (TAE) in the case where the local EP drive for TAE exceeds the stability limit. Based on quasilinear theory, the proposed 1.5D model assumes that the particles diffuse in phase space, flattening the pressure profile until its gradient reaches a critical value where the modes stabilize. Using local theories and NOVA-K simulations of TAE damping and growth rates, the 1.5D model calculates the critical gradient and reconstructs the relaxed EP pressure profile. Local theory is improved from previous study by including more sophisticated damping and drive mechanisms such as the numerical computation of the effect of the EP finite orbit width on the growth rate. The 1.5D model is applied on the well-diagnosed DIII-D discharges #142111 [M. A. Van Zeeland *et al.*, *Phys. Plasmas* **18**, 135001 (2011)] and #127112 [W. W. Heidbrink *et al.*, *Nucl. Fusion* **48**, 084001 (2008)]. We achieved a very satisfactory agreement with the experimental results on the EP pressure profiles redistribution and measured losses. This agreement of the 1.5D model with experimental results allows the use of this code as a guide for ITER plasma operation where it is desired to have no more than 5% loss of fusion alpha particles as limited by the design. © 2012 American Institute of Physics. [<http://dx.doi.org/10.1063/1.4752011>]

I. INTRODUCTION

Confinement of fusion-product alpha particles is crucial for sustaining ignition in next generation fusion devices as well as avoiding damage to the first wall. In ITER, as little as 5% of fusion products' power can be viewed as a limiting value for alpha particle loss.¹² Since the fusion product alpha particle velocities are comparable to Alfvénic velocities, they resonantly interact with Alfvénic modes which can lead to instabilities and large scale fast ion transport. In this paper, we propose a reduced version of the quasilinear model that computes the effect of this interaction on the fast ion profiles. A fully dimensional quasilinear model is currently being developed, while the present paper only deals with a 1.5D (1.5 dimensional) limit. We introduced the 1.5 dimensional term here to account for real space modification of the density profile and an added 0.5 for the modification of the velocity profile of fast ions that are in resonance.

To study the energetic particle interaction with Alfvénic modes, present day machines operate in regimes where the Alfvénic velocity, $v_A = B/\sqrt{4\pi n_i m_i}$, is comparable to that of the injected beams. Alfvénic modes can be strongly damped by the continuum. However, due to toroidicity, gaps in the continuum arise that allow discrete modes, such as toroidicity induced Alfvén eigenmodes (TAE), to exist and these waves have relatively small intrinsic damping when the driving energetic particles are absent. These discrete modes can be driven unstable by the free energy source of the energetic particles posing, therefore, a threat to energetic ion confinement.

Many present day experiments observe TAE activity with accompanying ion losses and profile relaxation.¹⁷ Under

some circumstances, a few modes expel fast ions from the plasma in bursts of activity. This was the case, for example, in the initial TAE experiments on TFTR¹⁶ and DIII-D.¹⁰ In these cases, fast-ion transport occurs in a burst cycle reminiscent of predator-prey models²⁶ that cannot be described by quasilinear models. In contrast, some contemporary experiments contain a large number of relatively small amplitude Alfvén instabilities. Examples include the TAE and “tornado” modes observed during ion cyclotron heating on TFTR,⁴⁰ JT-60U,²⁰ or JET²⁵ and the TAE and reverse shear eigenmodes (RSAE) activity observed during beam-heated reversed shear discharges in DIII-D.¹⁸ In the reversed shear plasmas, the hundreds of wave-particle resonances associated with the Alfvén instabilities flatten the fast-ion profile.²⁸ Modeling of these plasmas finds stochastic, diffusive transport over the affected region.²⁴ Under these circumstances, which may also govern fast-ion transport in ITER, a quasilinear model is expected to be reasonable. We compare the predictions of this proposed 1.5D quasilinear model through the comparison of losses in DIII-D's well-diagnosed discharges #122117²⁹ and #142111¹⁹ and achieve good correlation with the experimental results.

In Sec. II of this paper, we give an overview of the analytic theories that the proposed 1.5D model is based on. In Sec. III, we give a detailed description of the proposed model. We present the assumptions, approximations, and the method used to reconstruct the relaxed profiles of energetic particles interacting with TAE modes. Section IV is dedicated to presenting the experimental observations of the DIII-D shots we compare with the 1.5D model predictions. Finally, Sec. V presents the predictions of the 1.5D model on

the neutron deficit and EP profile redistribution in the DIII-D discharges #122117 and #142111.

II. MATHEMATICAL FRAMEWORK FOR FAST ION INTERACTION WITH TAE MODES

Interaction with TAE modes is speculated to be one of the major mechanisms for EP transport and potential loss.^{12,30,31} A qualitative description of the redistribution is as follows.

The growth rate of TAEs in the linear regime due to free energy of EPs is proportional to the gradient of EP pressure profile, $\gamma_L \propto \partial f / \partial r$. A TAE mode then grows at a rate $\gamma = \gamma_L - \gamma_d$, where γ_d is the linear damping rate, in absolute value, due to the background plasma. TAE modes then saturate when the pressure profile starts to flatten as a result of stochastic diffusion of particles. This flattening causes the growth rates to continue to diminish until it becomes comparable to the damping rate and then marginal stability is achieved. Here, we will assume that a steady turbulent state is achieved where a background mode spectrum enables stochastic diffusion of particles that arise from the steady state spectrum of TAE waves. Alternative scenarios where the spectrum is bursty or the modes do not produce mode overlap will not be considered in this paper.

In this section, we present the theoretical basis for the 1.5D model. The two main theories used to build the model are linear theory for the analytic expressions of the growth rate and the theory of quasilinear diffusion for the evolution of the wave particle system.

A. Linear theory

For the consistency of the presentation, we outline the derivation of the linear expression^{15,33} for the TAE mode growth rate that is used in the 1.5D model.

The condition for charge neutrality results in

$$\nabla \cdot \nabla \cdot \tilde{\mathbf{j}}_{\perp} + \nabla \cdot \left(\frac{\mathbf{B}_0}{B_0} \tilde{j}_{\parallel} \right) + \nabla \cdot \tilde{\mathbf{j}}^k = 0 \quad (1)$$

and the linearized momentum balance equation

$$-i\omega\rho_0\tilde{\mathbf{u}} = \mathbf{j}_0 \times \tilde{\mathbf{B}} + \tilde{\mathbf{j}}_{\perp} \times \mathbf{B}_0, \quad (2)$$

where \mathbf{B}_0 , \mathbf{j}_0 , and ρ_0 are the unperturbed magnetic field, current density, and mass density, respectively. $\tilde{\mathbf{j}}_{\perp}$ is the perturbed current density vector perpendicular to the magnetic field, \tilde{j}_{\parallel} is the component of the perturbed current density vector parallel to the magnetic field, $\tilde{\mathbf{j}}^k$ is the kinetically induced current density, and $\tilde{\mathbf{u}}$ is the fluid velocity which, from the ideal Ohms law, can be written as $\tilde{\mathbf{u}} = c(\tilde{\mathbf{E}} \times \mathbf{B}_0)/B_0^2$. The pressure gradient is ignored as a result of adopting the low-beta approximation valid for shear Alfvén problems.

Writing the perturbation in the electric field $\tilde{\mathbf{E}}$, magnetic field $\tilde{\mathbf{B}}$, and vector potential $\tilde{\mathbf{A}}$ as a function of the perturbed potential field $\tilde{\Phi}$ and assuming small scale perturbations across the field and long wave length perturbation along the field line, the above relations are used to obtain an eigenmode equation

$$\begin{aligned} & \frac{4\pi}{c} \left[\mathbf{B}_0 \times \nabla \left(\frac{\mathbf{B}_0 \cdot (\nabla \tilde{\Phi})}{B_0^2} \right) \right] \cdot \nabla \left(\frac{j_{\parallel}^0}{B_0} \right) \\ & + (\mathbf{B}_0 \cdot \nabla) \left(\frac{1}{B_0^2} \nabla \cdot \left[B_0^2 \nabla_{\perp} \left(\frac{\mathbf{B}_0 \cdot \nabla \tilde{\Phi}}{B_0^2} \right) \right] \right) \\ & + \nabla \cdot \left(\frac{\omega^2}{v_A^2} \nabla_{\perp} \tilde{\Phi} \right) = \frac{i4\pi\omega}{c^2} \nabla \cdot \tilde{j}^k. \end{aligned} \quad (3)$$

Due to periodicity in toroidal angle ϕ and poloidal angle θ as well as the independence of the equilibrium on ϕ , we can obtain a solution in the form,

$$\tilde{\Phi} = \sum_m \Phi_m e^{i(-m\theta + n\phi - \omega t)}. \quad (4)$$

Equation (3) is reduced to a set of coupled differential equations in Φ_m written as

$$\hat{L}_{ij}(\omega) X_j = 0, \quad (5)$$

where

$$X_i^{\dagger} = (\dots, \Phi_m, \Phi_{m+1}, \dots). \quad (6)$$

The operator, \hat{L}_{ij} , is written as the sum of the MHD operator $\hat{L}_{ij}^{(0)}$ and the kinetic response $\hat{L}_{ij}^{(1)}$

$$\hat{L}_{ij}(\omega) X_j = \left[\hat{L}_{ij}^{(0)} + \hat{L}_{ij}^{(1)} \right] X_j = 0, \quad (7)$$

where the right hand side of Eq. (3) is the kinetic response

$$\hat{L}_{ij}^{(1)} X_j = -\frac{4\pi i \omega}{c^2} \left(\frac{\partial}{\partial r} (r_j^k) - i m j_{\theta, m}^k \right). \quad (8)$$

This term is treated perturbatively to yield the damping and growth rates.

TAE modes are a solution to the MHD part of the equation, $L_{ij}^{(0)} = 0$. Assuming a form for the magnetic field $B_0 \approx 1 - \epsilon \cos \theta$, where $\epsilon = r/R$ results in the coupling of the two closest neighboring poloidal modes ϕ_i to $\phi_{j=i\pm 1}$. This reduces $L_{ij}^{(0)}$ to a tridiagonal matrix succinctly written as

$$\begin{pmatrix} P_m & Q \\ Q & P_{m+1} \end{pmatrix} \begin{pmatrix} \phi_m \\ \phi_{m+1} \end{pmatrix} = 0. \quad (9)$$

$P_m \phi_m = 0$ is the solution to an infinite cylinder whose result is the known Alfvénic dispersion relation $\omega = \pm k_{\parallel m}(r) v_A(r)$, where v_A is the Alfvénic velocity. The parallel wave vector is $k_{\parallel m} = \left(\frac{n}{R} - \frac{m}{Rq} \right)$, where $q = \epsilon B_{tor}/B_{pol}$ is the safety factor. The frequencies of the neighboring poloidal modes overlap at $k_{\parallel m}(r_m) = -k_{\parallel(m+1)}(r_m)$ at r_m such that $q(r_m) = (m + \frac{1}{2})/n$.

Due to the toroidal coupling from Q , the degeneracy is lifted, and a gap in the continuum is formed at r_m . This is akin to electron bands forming in solids due to Bragg's diffraction.

Within these gaps lie isolated TAE modes that are hardly damped by the continuum and could be subject to a strong drive from the wave-particle interaction due to the

kinetic response in Eq. (8). TAE modes are the isolated eigenmode solutions to Eq. (7). The drive is manifested as an imaginary component to the eigenvalue solution computed perturbatively as follows:

$$\frac{\gamma}{\omega} = - \frac{\int_0^a r dr X_i^{(0)} \overline{L_{ij}^{(1)} X^{(0)}}}{\int_0^a r dr X_i^{(0)} \partial L_{ij}^{(0)} / \partial \omega X_j^{(0)}}. \quad (10)$$

where the overline denotes the flux surface averaging of the quantity within $\bar{x} \equiv (2\pi)^{-1} \int (1 + \epsilon \cos(\theta)) x d\theta$. As further discussed in Sec. III C, Eq. (10) is expanded in the different limits to give analytic forms for the local damping and growth rates that the 1.5D model uses.

B. Quasilinear theory

To study the effect of TAE modes on the EP distribution function in the framework of quasilinear theory, the second order perturbation, $f^{(1)E(1)}$, is maintained in Vlasov's equation. This results in a diffusion like equation for the ensemble averaged EP distribution function f .³⁶ The mode's amplitude evolves at a rate $\gamma_k = \gamma_L - \gamma_d$, where γ_L is the instantaneous linear growth rate that depends on the EP distribution function; and γ_d is the damping rate, in absolute value, that depends on the background plasma. This is depicted in the following set of coupled equations:

$$\frac{\partial f}{\partial t} = \pi \sum_k \left(\omega \frac{\partial}{\partial E} + n \frac{\partial}{\partial P_\phi} \right) D_k \left(\omega \frac{\partial}{\partial E} + n \frac{\partial}{\partial P_\phi} \right) f, \quad (11)$$

$$\frac{dW_k}{dt} = 2(\gamma_L - \gamma_d)W_k, \quad (12)$$

$$\gamma_L = \frac{\pi}{2} \int_c^q dP_\phi dE \left| \left\langle \frac{v_d \cdot \delta E}{\omega} \right\rangle \right|^2 \delta(\Omega) \left(\omega \frac{\partial}{\partial E} + n \frac{\partial}{\partial P_\phi} \right) f, \quad (13)$$

where $D_k = W_k \left| \left\langle \frac{q}{c\omega} v_d \cdot \delta E \right\rangle \right|^2 \delta(\Omega)$ is the diffusion coefficient at the resonances in phase space; W_k is the square of the mode amplitude; v_d is the particle drift velocity; $\Omega(P_\phi, E, \mu) = \omega_{TAE} - n \langle \omega_\phi \rangle + l \langle \omega_\theta \rangle$, where $\langle \omega_{(\theta, \phi)} \rangle$ are the drift orbit averaged toroidal and poloidal bounce frequencies of the particles. $E = Mv^2/2$ is the energy of the particle and $P_\phi = MRv_\parallel - (e/c)\Psi(r)$ is the canonical angular momentum where v_\parallel is the parallel velocity of the fast ions and $\Psi(r) = \int r' B/q(r')$, R is the major radius, e and M are the particle charge and mass, respectively.

Knowing the equilibrium profiles of the plasma, it is possible to find all the resonances in phase space, $\Omega(P_\phi, E, \mu) = \omega_{TAE} - n \langle \omega_\phi \rangle + l \langle \omega_\theta \rangle = 0$, and solve the self consistent equation, Eq. (11), to compute the evolution of the mode amplitude and resultant relaxation of the profile.¹⁴ This will be the subject of future work. In the current paper, we discuss the reduced 1.5 dimensional version of this model.

III. 1.5D MODEL

In this section, we describe the approximations and modeling made that allow for reduction of the quasilinear

theory of diffusion to a 1.5 dimensional model. Then, we give a detailed description of the 1.5D model and the method for integrating the relaxed profiles. Finally, we give an account of the analytic growth/damping rates that are used.

A. Assumptions and approximations

1. Radial redistribution only

The assumption $\omega_{*EP} \gg \omega_{TAE}$, where ω_{*EP} is the mean drift frequency of the energetic particles, is taken everywhere. This entails that significant diffusion takes place only in P_ϕ or the radial direction and transport in E or v direction is neglected. The 1.5D model is developed to find the resulting relaxation of the EP pressure profile in the radial direction. In full dimensionality, the diffusion coefficient D_k , introduced in Sec. II B, is a function of all the phase space variables. Since we are interested in the diffusion coefficient as a function of radius only, we are concerned with the radial dependence of D_k , denoted by $D(r)$ in what follows.

2. Accounting for phase space relaxation

Since the pressure profiles are obtained by integrating the distribution function over the velocity, we use Kolesnichenko's calculations³⁷ to find the ratio of particles, η , that are in resonance with the TAEs. It is roughly estimated for two cases, alphas and beams, as follows:

$$\eta = \frac{(v_{\alpha 0} - v_\parallel) v_\parallel}{v_{\alpha 0}^2} \quad \text{for alpha distributions,} \quad (14)$$

$$\eta = \frac{v_\parallel^2}{v_{b0}^2} \quad \text{for beam-like distributions.} \quad (15)$$

This means that only an η fraction of fast ions relax, while $1 - \eta$ of them remain unchanged. Fig. 1 illustrates the resonant region part in phase space.

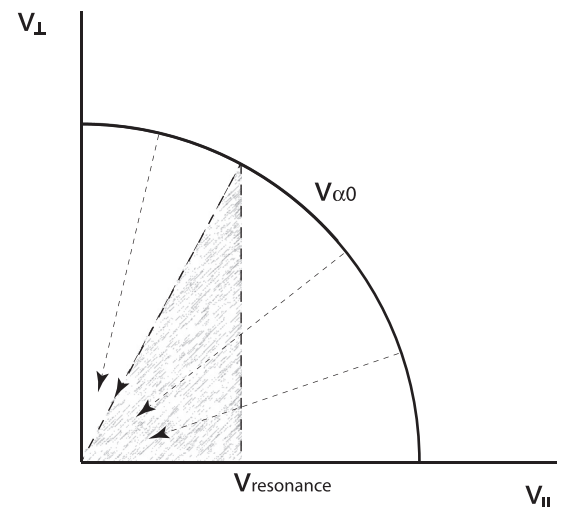


FIG. 1. Depiction of the resonant and non-resonant regions of phase space for finding the contribution of the velocity to the redistribution of energetic particles.

3. Local growth and damping rates

We make use of local expressions for the growth and damping rates of TAEs, while the modes are, in actuality, global. Therefore, the use of a comprehensive code such as NOVA-K⁹ is required. Then the values of the damping and growth rate computations are used to normalize the rates. Having the damping and growth rates normalized in this manner, we maintain their analytically computed dependence on the plasma parameters. This way the entire 1.5D quasilinear model is expected to describe the expected functional dependencies correctly. In addition, the rates are averaged over the linear eigenmode width, Δ_m , to account for the spatial breadth of the mode.

4. Instant radial transport

We do not consider the transition time period in which the mode and the distribution both evolve with time. Instead, it is assumed that the quasilinear equations will bring the mode to a marginal stability state, and a near steady state distribution function and fields will be achieved to bring about a steady state, $D(r) \rightarrow 0 \Rightarrow \partial f(r, t)/\partial t = 0$. This happens as a result of fast ion diffusion relaxation in all unstable regions of phase space, which diminishes the gradient in the EP pressure profile until the plasma state $\gamma_L \leq \gamma_d$ is achieved everywhere.

B. Integrating the relaxed profile

Assuming that the background plasma remains unaffected, the local damping rates are unchanged. We calculate the estimated local critical EP pressure gradient by balancing the TAE drive to the most important damping mechanisms. TRANSP⁶ provides the pressure profiles, established by classical relaxation processes (which when unstable will relax to marginal stability profiles in accord with 1.5D assumptions) as well as any other equilibrium plasma quantity needed in the 1.5 D calculation.

The analytic expressions for growth^{3,33} and damping^{7,21,34,39} rates assume the existence of a multitude of TAEs centered at all radial positions. Each of these radially localized modes has rates that depend on the mode numbers n , m , and other local plasma quantities. This will be detailed in Sec. III C.

Many modes can exist at every radial location, but we are interested in finding the growth rate of the most unstable one which is theoretically predicted⁴ to be around $\rho_{EP} k_{\perp} \approx 1$, where ρ_{EP} is the particle orbit width due to cross field drift.

It is shown that there is a plateau³⁸ in the growth rate as a function of toroidal mode number n for which γ_L is maximized at a given radial location

$$\frac{r^2 \omega_c}{R q^2 v_A} \approx n_{min} < n < n_{max} \approx \frac{r \omega_c}{q^2 v_A}, \quad (16)$$

where ω_c is the EP cyclotron frequency, q is the safety factor, and v_A the Alfvénic velocity. The growth rate chosen at a given radius is that of the mode whose n number satisfies

Eq. (16). The poloidal mode number m is related to n through $q(r) = (m + 1/2)/n$. This specifies the mode for which the rates are computed at a given radial location.

For each mode, the absolute value of the local linear damping rate, γ_d , is assumed fixed since it depends on the unaffected background plasma, while the mode's growth rate γ_L is a function of the gradient of the EP pressure which undergoes relaxation in the presence of TAEs. In regions where the mode is unstable, $\gamma_L > \gamma_d$, the gradient diminishes as energetic particles diffuse due to their resonant interaction with TAE modes. Assuming that the transport is strongest in the P_{ϕ} , i.e., radial direction, as would be the case for $\omega_{*E} \gg \omega$, we neglect any transport in the E direction. Therefore, we express the growth rate as a function of the radial gradient in EP pressure profile, $\gamma_L = \gamma'_L \partial \beta / \partial r$, where γ'_L is independent of EP profiles.

At marginal stability, the gradient assumes a critical value such that the growth rate equals the damping rate, $\gamma_d = \gamma'_L (\partial \beta / \partial r)_{crit}$. The unperturbed plasma profiles are computed using equilibrium codes such as TRANSP, from which we calculate γ_d everywhere and compute γ'_L . This is used to calculate the critical value of the EP gradient

$$\left. \frac{\partial \beta_{EP}}{\partial r} \right|_{crit} = \frac{\gamma'_L}{\gamma_d}. \quad (17)$$

Note how the right hand side of Eq. (17) is independent of β_{EP} and only depends on the unchanged background plasma.

In the 1.5 dimensional quasilinear diffusion equation, $D(r)$ grows at a rate proportional to $\gamma_L - \gamma_d$. This results in diffusion of particles in the unstable region, where $D(r) > 0$. The changing radial profile leads to an increased instability drive that extends the unstable region into neighboring regions that were originally stable. Particles continue to undergo diffusion in the unstable region, until $\partial \beta_{EP} / \partial r$ decreases to the point where $\gamma_L \leq \gamma_d$. The relaxed β profiles are integrated assuming the critical value of the gradient in beta, $\partial \beta / \partial r|_{crit}$, in regions of TAE instability $[r_1, r_2]$, where $\partial \beta_{EP} / \partial r > \partial \beta_{EP} / \partial r|_{crit}$ and maintain the original value in regions that are stable. To insure the continuity and the conservation of particles, we extend the boundaries of the unstable region to $[r_-, r_+]$ iteratively until both conditions, continuity and particle conservation, are satisfied. As a result, the pressure profile is modified over a region larger than the initially unstable region. This is a feature that was realized in the pioneering work in quasilinear theory.^{11,41}

For the purpose of illustration, we show in Fig. 2 an example of the redistribution resulting in a profile $f(r)$ with the corresponding critical gradient $\partial f / \partial r|_{crit}$ everywhere. The following calculation is done using the 1.5D model integration scheme described above for an arbitrary $f(r) = (1 - r^2)^{5/2}$ and arbitrary critical gradient $\partial f(r) / \partial r|_{crit} = 20(2r - 0.8)(r - 0.6) + 0.6$, where, $r = [0, 1]$.

This mechanism agrees with the quasilinear theory of diffusion in which regions of instability extend into originally stable regions as particles diffuse into them. A similar effect is known to be significant in the plasma turbulence area.³⁵

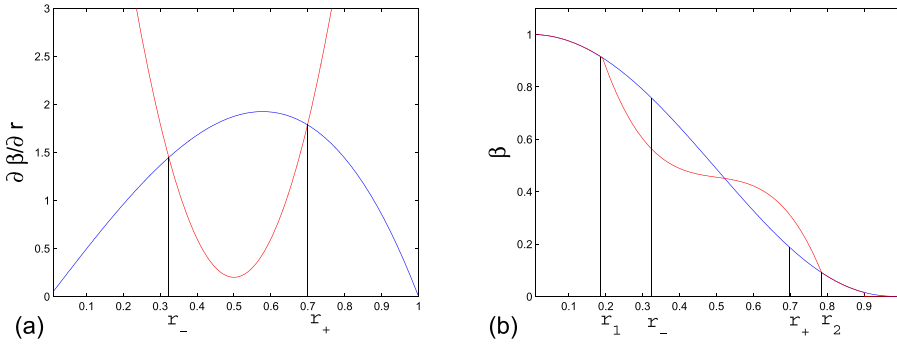


FIG. 2. An illustration for the integration scheme of 1.5D. (a) The values for the original gradient in pressure profile (blue) and the critical gradient (red). $[r_-, r_+]$ is the original region of instability where $\partial\beta/\partial r > \partial\beta/\partial r|_{crit}$. (b) The original pressure profile (blue) and the relaxed profile (red). The redistribution has extended into the region $[r_1, r_2]$ which is larger than the originally unstable region $[r_1, r_2]$.

One can see how, in 1.5D, this behavior is captured without the detailed calculation of the perturbed fields that produce this diffusion coefficient. Therefore, 1.5D is capable of quickly and efficiently predicting an estimate of the amount of redistribution and transport of energetic particles.

C. Growth and damping rates

For TAE modes to be excited, the mode's growth rate must be larger than the sum of all damping rates. NOVA simulations indicate that the different damping mechanisms are of varying importance depending on the fusion device and the plasma parameters. It has been found for typical parameters projected for ITER^{2,8,14,21,32,39} that ion Landau damping and radiative damping are predominant with the electron collisional damping negligible. On the other hand, in the DIII-D experiments investigated here, radiative and electron collisional damping are the main damping mechanisms. Unlike the rest of the damping mechanisms, radiative damping is non-perturbative.

1. Radiative damping

Radiative damping results from the coupling of short wavelength kinetic Alfvén waves (KAW) to TAE mode. It is typically computed when finite Larmor radius effect (FLR) and electron pressure perturbations are used to extend the second order differential equation structure to the fourth order. In NOVA, it is computed perturbatively.^{1,22} The dissipation of these short wavelength KAWs leads to finite damping of TAE modes.

The following expression³⁹ is used

$$\frac{\gamma_{rad}}{\omega} = -3 \left| \frac{\sqrt{\rho^2} sm(m+1)}{r\sqrt{2} 2m+1} \right|^{0.67}, \quad (18)$$

where s is the local shear at the location of the mode, m is the poloidal mode number and $\rho = v_s/\omega$ with v_s the speed of sound, and ω is the ion gyro-frequency.

The following damping mechanisms are derived perturbatively from linear theory using Eq. (10).

2. Ion Landau Damping

The following expression⁵ derived for kinetic response due to the collisionless interaction of the background ions is

$$\frac{\gamma_{iL}}{\omega} = -\frac{q^2 \sigma \sqrt{\pi}}{18(1 + \sigma/4)} x_i^3 e^{-x_i^2}, \quad (19)$$

where σ is the plasma ion depletion factor, $\sigma = n_i/n_e$ and $x_i = v_A/3v_i$.

3. Electron Landau damping

The analytic expression for the damping rate resulting from the collisionless interaction of the background electrons is derived by Candy⁷ in the limit of low beta, large aspect ratio. The expression is

$$\frac{\gamma_{eL}}{\omega} = -\frac{\pi^{3/2}}{6} q^2 \beta_e \frac{v_A}{v_e} \left(\frac{5}{2} \epsilon \right) G(\hat{\epsilon}) e^{1/s}, \quad (20)$$

with $G(\hat{\epsilon}) \approx 447 - 042\hat{\epsilon} + 0.02\hat{\epsilon}^2$; s is the local shear, β_e is the electron β , and $\hat{\epsilon} = 2\epsilon/(1 - \epsilon)$.

4. Electron collisional damping

The electron kinetic response³⁴ affects the TAE modes through the perturbation in their distribution function resulting from collisional damping with electrons. Since $v_{Te} \gg v_{Ti}$, only electrons with velocities $v_{||} \ll v_{Te}$ would interact with the Alfvén modes. Therefore, the main contribution comes from trapped particles where $v_{||} \ll v_{\perp}$. The expression²¹ for the resulting damping rate is

$$\frac{\gamma_{eColl}}{\omega} = -\frac{1}{4} \left[I_1 \left(\frac{8snq\rho_s}{5r\epsilon} \right)^2 + I_2 q^2 \frac{8\beta_{pc}}{1 + \sigma} \right] \sqrt{\frac{\nu}{\omega}} \times \left[\ln \left(16 \sqrt{\frac{\omega\epsilon}{\nu}} \right) \right]^{-3/2}, \quad (21)$$

where β_{pc} is the core plasma β , $I_1 = (0.43Z_{eff} + 1.06)$, and $I_2 = (1.03Z_{eff} + 2.3)$, with $Z_{eff} = 6 - 5\sigma$ and the electron collision frequency

$$\frac{\nu}{\omega} = \frac{4\pi n_e e^4 \ln \Lambda_e}{\omega m_e^2 v_{Te}^3}. \quad (22)$$

5. Growth rate

The main mechanism for the TAE drive is provided by the free energy from the gradient in the energetic particle distribution. Using the linear theory, one can find the perturbed EP distribution function, \tilde{f} , from which the current density is

evaluated, $\tilde{j} = \int d^3v v f$. The energetic particle kinetic response is thus calculated and different expressions can be derived for various limits, such as passing and trapped or whether $\Delta_m \ll \Delta_b$ or vice-versa. The expression is only valid in the limit where $\rho_\alpha \ll \Delta_m$, where ρ_α the fast ion gyroradius.

To find the kinetic response of the energetic particles, the drift kinetic equation is used to write the analytic form³³ for the growth rate.

D. Normalizing with NOVA-K

We use the above analytic expressions for computing the local growth and damping rates of the TAE modes at all radial positions. For a quantitatively accurate representation, we calibrate them to values computed by the established code, NOVA-K. This procedure allows for more accurate application of the 1.5D model on experiments such as DIII-D.

The NOVA-K code computes exactly the TAE growth rate, including effects coming from TAE mode structure, finite Larmor radius, and drift orbit radial width. It also computes the damping rates. This is an area being successfully investigated by the ITPA working group.¹³ We describe here how a specific procedure is developed in order to include the finite orbit width effect in the drive. First, we use the NOVA code to find several mode structures localized at different radii. To simplify the NOVA study, we focus on only one toroidal mode number, which is taken at a value approximately corresponding to the maximum (plateau region) value of the growth rate as a function of the ratio Δ_m/Δ_b . Our goal here is to evaluate the growth rate in the plateau regime, which would give the required approximation for the TAE-like mode growth rate for the 1.5D model we develop here. However, because of the finite value of n , we expect that it is unlikely that we hit the maximum of the growth rate plateau. Instead of going through the different choices of n numbers, we change z_{EP} , the particle charge. Note that in the expression for the drive, the particle's charge enters only through the combination n/z_{EP} . Thus, with the fixed n value, we can find the plateau regime by changing z_{EP} and finding the growth rate of the most unstable mode. This procedure is robust since the plateau regime is found regardless of whether we use n or $n + 1$ and vary z_{EP} in the search.

For the application of 1.5D on DIII-D results, we use a two point normalization scheme, where we find the most unstable modes localized at two radial points. One is relatively close to the center of the plasma, $r_1 \approx 0.3a$ and one is towards the edge, $r_2 \approx 0.7a$, where a is the minor radius. The analytically computed rates are modified by a constant multiple $g_1 = \gamma_{1(NOVA)}/\gamma_{anlt}(r_1)$ for $r < r_1$ so that it coincides with the value of the NOVA-K computed one at r_1 . The procedure is identical for $r > r_2$ which is multiplied by $g_2 = \gamma_{2(NOVA)}/\gamma_{anlt}(r_2)$, where $\gamma_{1,2(NOVA)}$ are the NOVA computed rates of the modes around $r_{1,2}$. For $r_1 < r < r_2$, the rate is multiplied by a linear function $ar + b$ such that $ar_1 + b = g_1$ and $ar_2 + b = g_2$.

For robustness, we build the code such that the input for normalization can be in two forms. On one hand, the input is the normalization constant at two given radial positions from which $g(r)$ is directly known and multiplies the analytic rates. This allows for the use of the same normalizations for multi-

ple times of interest for the same discharge, such as in the following case of #127111 for $t > 600$ ms. Alternatively, the input can be NOVA-K values for the rates at two given radial positions from which the normalization constants are then computed and in turn used on the analytic profiles. This is done when analyzing specific times distinctly as in #142111 and for # 122117 at $t < 600$ ms as will be described later.

E. Computing losses

To account for the losses of particles, the condition for the conservation of particles is lifted once the region of instability grows large enough to result in particle loss at the edge. While integrating for the relaxed profiles according to the method discussed in Sec. III B, fast ions are lost when the boundary r_+ reaches the loss boundary, $r_b = a - \Delta_f/2 + \rho_f$, where a is the minor radius, $\Delta_f = q\rho_f$ is the estimate for the fast ion orbit width, and ρ_f is the fast ion Larmor radius. The profile is then integrated with $r_+ = r_b$ and the fraction of lost particles is computed as follows:

$$L = \frac{\int_0^a dr (\beta_{rlx}(r) - \beta_{ini}(r))}{\int_0^a dr \beta_{ini}(r)}. \quad (23)$$

To compare with the experimental observation of the neutron rate depletion, we calculate the fraction of the neutrons expected with the relaxed profile to that expected from the initial profile using the cross section $\langle \sigma v \rangle$ as derived from TRANSP. The following is the expression used

$$L_n = \frac{\int_0^a \langle \sigma v \rangle \beta_i \beta_{rlx}}{\int_0^a \beta_i \beta_{ini}}, \quad (24)$$

where β_i is the ion pressure, β_{ini} is the initial beam pressure, and β_{rlx} is the pressure of the relaxed beam. Even if energetic particles are not lost to the wall, the mere modification in their β profile due to redistribution can result in a change in the neutron rate albeit less significantly.

IV. OBSERVED DIII-D FLATTENING

A series of DIII-D experiments^{10,18,27} has been conducted to investigate TAE activity and Alfvén eigenmode (AE) induced fast ion transport. It has been observed that a rich spectrum of TAE and RSAE (also called Alfvén Cascade modes) is produced when high energy neutral beams are injected into the reversed shear plasmas. We look at two discharges that have been extensively diagnosed and analyzed, discharge # 122117 and discharge # 142111, where AE activity has been associated with significantly flattened fast ion pressure profiles and losses.

The first discharge shows the presence of strong TAE and RSAE modes and resulting losses which are captured by 1.5D. The second discharge is of special interest, since during the time span of the discharge, TAE/RSAE activity is significantly reduced until the instability becomes marginal

at some point. This provides a sensitive test for theoretical models, such as the 1.5D model developed here.

A. Diagnostics

Alfvénic activity is detected with a suite of fluctuation diagnostics that are sensitive to Alfvénic instability oscillations. Electron temperature is measured with electron cyclotron emission (ECE). CO₂ interferometer, beam-emission spectroscopy, and reflectometers are used for measuring the density fluctuations, and Mirnov coils are used to measure the magnetic fluctuations.

As for the fast ion diagnostics, there are four main diagnostics used.

Plastic scintillator is used to measure the volume averaged neutron emission rate which is predominantly due to plasma-beam interaction making it a direct function of the energetic particle pressure profiles.

FIDA is a charge exchange recombination spectrometer technique that uses the Doppler-shifted Balmer- α light emitted by fast ions. This is used to measure the fast ion profile.

MSE is a diagnostic that depends on the motional Stark effect to find the internal magnetic fields. The total pressure is computed using MHD equilibria obtained and the measured MSE magnetic fields. Subtracting the plasma pressure (computed using measured temperature and density profiles) from this total pressure results in the fast ion pressure profile.

FILD is a scintillator based fast ion loss detector²³ inserted just outside the last closed flux surface to detect fast ions over a large region of the phase space, (E, μ) , where E is the energy and μ is the pitch angle.

B. Experimental Observation

We present an overview of the experimental results for discharges # 122117 and #142111 that will be used to validate the 1.5D model. The results presented here on experiments are adapted from works of Heidbrink²⁹ and Van Zeeland.¹⁹

1. Discharge # 122117

At the baseline shot #122117, a deuterium neutral beam injection (NBI) is injected with $P_{NBI} = 4.6$ MW, $E_{b0} = 80$ keV, at a tangency radius of 1.15 m. The peak of the energetic particle distribution is around $v_{||}/v = 0.68$. AE activity is detected using the diagnostics described in Sec. IV A and depicted in Fig. 3 below. The EP detectors reveal flattening in the profiles around the center at all times of interest shown in Fig. 4. Neutron deficits like those observed in #122117 can be a result of fast ion redistribution to larger radii as well as fast ion loss. Our simulations (which will be discussed in Sec. V) show that early during the discharge, there is a combination of EP losses and redistribution in phase space while later during the current ramp, the EP is predominately redistributed without losses resulting from particle transport beyond the last closed flux surface.

2. Discharge #142111

Another well diagnosed discharge is #142111.¹⁹ The on-axis magnetic field for this discharge is $B_T = 2$ T, and the

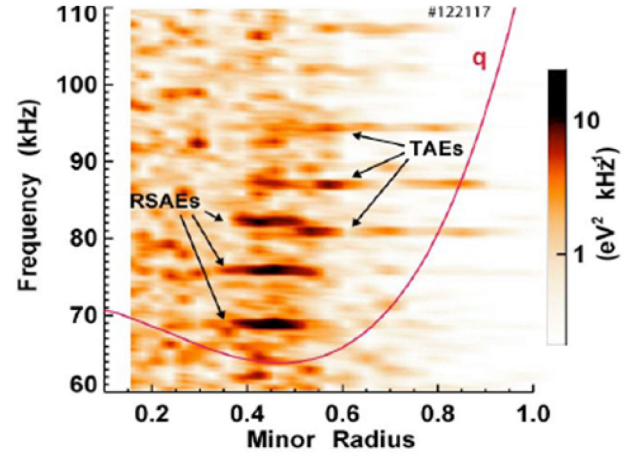


FIG. 3. Radial profile of ECE radiometer power spectrum depicting the observed TAE and RSAE activity in DIII-D discharge # 122117 at $t = 410$ ms. The solid line is the safety factor profile, q . These measurements depict the existence of AEs around the minimum of q and extending to $r/a = 0.8$. Adapted from Ref. 18. Adapted from M. A. Van Zeeland, Phys. Rev. Lett. **97**, 135001 (2006). Copyright (2006) American Physical Society.

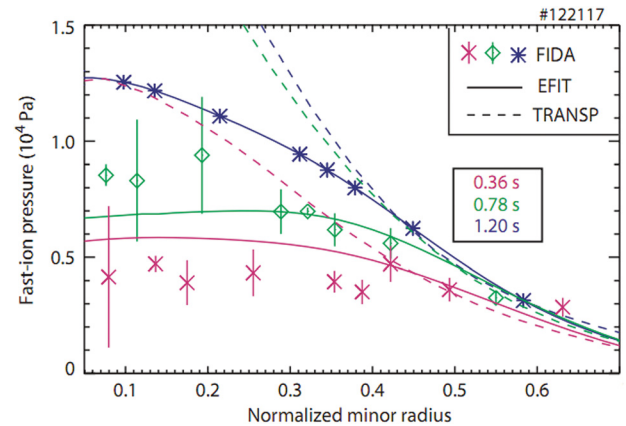


FIG. 4. A depiction of the unperturbed profiles from TRANSP in dashed lines of different colors for the times, $t = 360$ ms, $t = 780$ ms, and $t = 1200$ ms. The profiles are modified due to interaction with TAE activity depicted in Fig. 3 and the FIDA measurements are presented as dots while the MSE fit is in solid lines. Reprinted with permission from W. W. Heidbrink *et al.*, Nucl. Fusion **48**, 084001 (2008). Copyright 2008 IOP Publishing Ltd.

current increases at a rate 0.8 MA/s until it reaches 1.2 MA at $t = 1000$. 80 keV neutral beams are injected at $t = 300$ ms with a total power of 6.8 MW. Fig. 5 shows the AE activity as a function of time and the associated EP coherent losses detected by FILD. Note that the FILD detected coherent losses correspond primarily to TAE frequencies.

V. COMPARISON OF 1.5D RESULTS WITH THE OBSERVED DIII-D BEAM ION FLATTENING

The extensive DIII-D experiments that are dedicated to the study of AEs and their interaction with energetic particles readily lend themselves for validation of EP transport models and numerical simulations. The most notable discharges, # 142111 and # 122117, are used here to validate the proposed 1.5D model.

TRANSP provides the machine and plasma parameters such as the major radius R , minor radius a , and on-axis

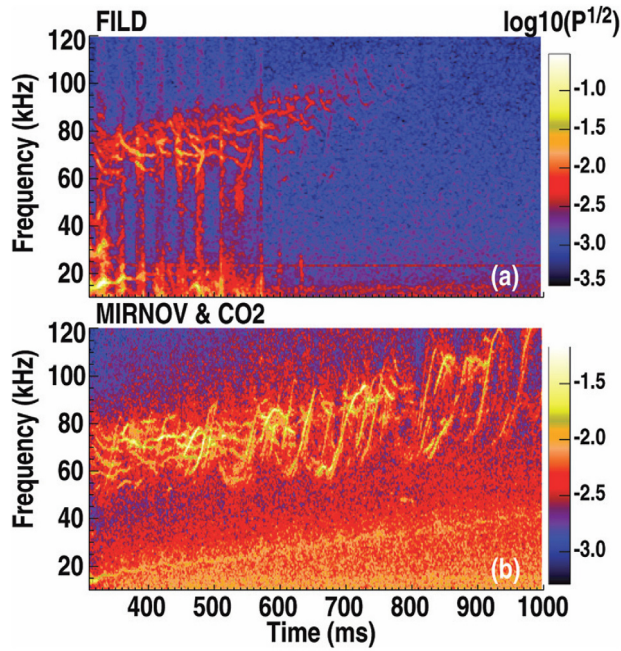


FIG. 5. (a) FILD activity signifying coherent NBI loss peaking around $t=500$ ms and disappearing after $t=800$ ms. (b) AE activity measured throughout the discharge in the spectrum of Mirnov and CO_2 interferometer data. Adapted from Ref. 19. Adapted from M. A. Van Zeeland, Phys. Plasmas **18**, 056114, (2011). Copyright 2011 American Institute of Physics.

magnetic field B , as well as the plasma and beam profiles. The profiles used for this 1.5D model are the ion temperature, $T_i(r)$, electron temperature, $T_e(r)$, plasma pressure $\beta_{pc}(r)$, beam pressure, $\beta_{bm}(r)$, electron pressure, $\beta_e(r)$, ion density $n_i(r)$, and the safety factor, $q(r)$. Once these parameters and profiles are accessible, the analytic linear growth and damping rates, as discussed in Sec. III C, are easily calculated for the most unstable mode at each radial position. These rates are then calibrated to NOVA-K computed linear rates using a normalization scheme described in Sec. III D.

A. NOVA-K simulations

Due to its crucial role in determining the results of 1.5D on experimental data, we present the NOVA-K computed

eigenmodes and their linear growth and damping rates used to normalize the analytically computed rates of two discharges analyzed. We use a two point normalization scheme, which entails finding two modes and their rates for each case we analyze. The procedure is discussed in details in Sec. III D.

1. Discharge #122117

We use results of NOVA-K simulations for the rates at two radial positions to normalize the analytically computed rates as a function of radius. The safety factor measurements have been optimized for $t < 600$, so we choose to use NOVA-K at $t=360$ and $t=410$ to compare the model's predictions for neutron losses with the experimentally detected ones. However, since FIDA results for later times, $t=780$ ms and $t=1200$ ms also exist, we use the rates computed by NOVA-K at $t=360$ ms to normalize later times where we also model TAE-EP interaction using 1.5D. For the purpose of illustration, we present in Fig. 6 the mode structures of the TAE modes computed by NOVA for discharge #122117 at $t=360$ ms. However, we present the rates computed for both $t=360$ ms and $t=410$ ms for which NOVA-K was used.

The computed linear growth and damping rates:

For $t=360$

Mode location	$\gamma_{\text{growth}}/\omega$ (%)	$\gamma_{\text{eColl}}/\omega$ (%)	$\gamma_{\text{rad}}/\omega$ (%)
$r/a=0.32$	11	2	0.3
$r/a=0.78$	1.7	3	0.2

For $t=410$

Mode location	$\gamma_{\text{growth}}/\omega$ (%)	$\gamma_{\text{eColl}}/\omega$ (%)	$\gamma_{\text{rad}}/\omega$ (%)
$r/a=0.23$	26	0.1	1.4
$r/a=0.75$	4.1	0.09	8.8

When there is continuum damping, we add it to the radiative damping. This was the case for $t=410$.

NOVA is a perturbative ideal MHD code⁹ that solves in matrix form a reduced set of second order differential equations in $\xi(\rho)$, the vector of amplitudes of poloidal harmonics of the radial displacement as a function of $\rho \equiv \sqrt{\psi/\psi_0}$, and the square root of the normalized poloidal field flux. However, it is possible that the numerical solution propagates into the continuum and still has finite

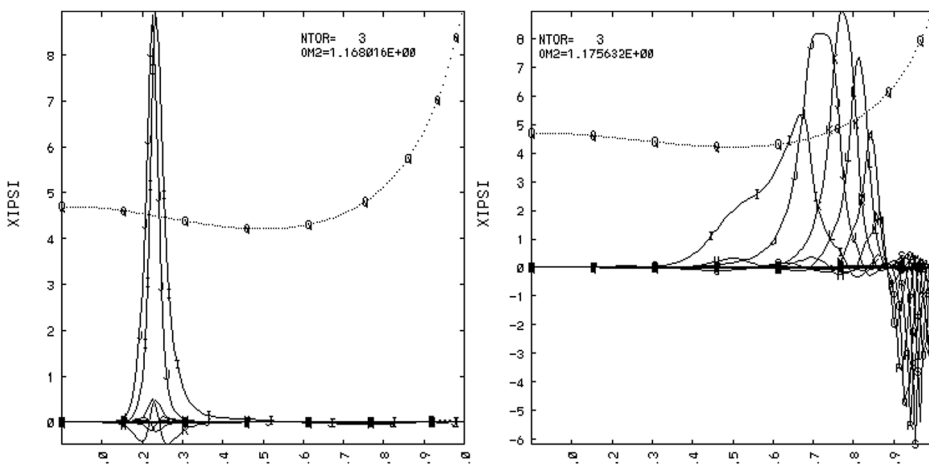


FIG. 6. The structure of modes localized around $r=0.32$ and $r=0.78$ for shot # 122117 at $t=360$ ms as computed by NOVA for $n=3$. The modes are computed as a function of $\sqrt{\psi/\psi_0}$, the square root of the normalized poloidal field flux. The dotted line is the safety factor profile.

Fourier components. It is an approximation but it is consistent with expectations from ideal MHD. This results in a jump in the imaginary part of the eigenmode structure giving rise to the continuum damping. However, since this procedure only provides the real part of the eigenvalue for the singular TAE mode, the flux function $\hat{C}(d\xi/d\rho)$, which is continuous around the resonance with the continuum, is introduced²² to find the effect of the interaction with the continuum. The MHD equations written in terms of flux function are not singular and one can use the perturbative technique to find the complex correction resulting from the interaction of the mode with the continuum. The details are found in Gorelenkov's treatment.²²

2. Discharge #142111

For this discharge, the safety factor measurements have been optimized for $t = 425, 525, 675, 725, 800,$ and 975 ms. Therefore, NOVA-K simulations are made at all these times to compare the model expectations with the experimental results. To avoid redundancy, we only show the mode structures (Fig. 7) of the $t = 675$ ms for discharge #142111, while presenting the rates of the most unstable modes at two given radii for all the times analyzed.

The computed NOVA-K linear growth and damping rates:

For $t = 425$			
Mode location	$\gamma_{\text{growth}}/\omega$ (%)	$\gamma_{\text{eColl}}/\omega$ (%)	$\gamma_{\text{rad}}/\omega$ (%)
$r/a = 3$	8.23	0.6	1.8
$r/a = 0.82$	0.37	2.2	0.733
For $t = 525$			
Mode location	$\gamma_{\text{growth}}/\omega$ (%)	$\gamma_{\text{eColl}}/\omega$ (%)	$\gamma_{\text{rad}}/\omega$ (%)
$r/a = 0.23$	11	0.16	1.8
$r/a = 0.83$	4.9	0.29	0.67
For $t = 675$			
Mode location	$\gamma_{\text{growth}}/\omega$ (%)	$\gamma_{\text{eColl}}/\omega$ (%)	$\gamma_{\text{rad}}/\omega$ (%)
$r/a = 0.25$	22	0.15	3.5
$r/a = 0.75$	4.9	0.16	2.7

For $t = 725$

Mode location	$\gamma_{\text{growth}}/\omega$ (%)	$\gamma_{\text{eColl}}/\omega$ (%)	$\gamma_{\text{rad}}/\omega$ (%)
$r/a = 0.3$	56	0.11	1.3
$r/a = 0.85$	3.1	2.7	1.3

For $t = 800$

Mode location	$\gamma_{\text{growth}}/\omega$ (%)	$\gamma_{\text{eColl}}/\omega$ (%)	$\gamma_{\text{rad}}/\omega$ (%)
$r/a = 0.2$	12.5	0.21	2.9
$r/a = 0.8$	3	0.11	1.9

For $t = 975$

Mode location	$\gamma_{\text{growth}}/\omega$ (%)	$\gamma_{\text{eColl}}/\omega$ (%)	$\gamma_{\text{rad}}/\omega$ (%)
$r/a = 0.2$	1.8	0.8	0.052
$r/a = 0.8$	2.2	18	0.44

B. 1.5D results

To implement the 1.5D model on the DIII-D shots of interest, Eq. (10) is expanded in the limit of highly anisotropic passing particles with consideration for the finite orbit width. The expression therefore depends on the ratio Δ_b/Δ_m , where $\Delta_b = q\rho_b$ is the beam width with q the safety factor, ρ_b is the EP Larmor radius, and $\Delta_m \approx r_m/m$ is the mode width with r_m the location of the TAE mode, and m the poloidal mode number. Using local expressions for the case of the two discharges being analyzed, the value of Δ_b varies between 5 and 20 cm, while Δ_m is around 2 cm. Therefore, we use the following analytic expression^{3,33} for the growth rate expanded in the limit of $\Delta_b \geq \Delta_m$:

$$\frac{\gamma}{\omega} = -q_m^2 \beta_b^p \frac{\omega_*^p}{\omega_r} (1 + \chi_0^2)^2 \times 24 \frac{\Delta_m^3}{\xi_p^3} \sum_{s=\pm 1} y_s \theta(1 - y_s), \quad (25)$$

where θ is the step function; q is the value of the safety factor at the mode location; ω_* is the local diamagnetic frequency; χ_0 is the pitch angle; $\xi = (1 + \chi_0^2)qv_0/(\chi_0\omega_c)$; and $y_s = v_A/(|2s - 1|\chi_0 v_0)$.

1. Discharge #122117

We compute the critical value of the gradient in beam pressure profiles of discharge #122117 that would result in

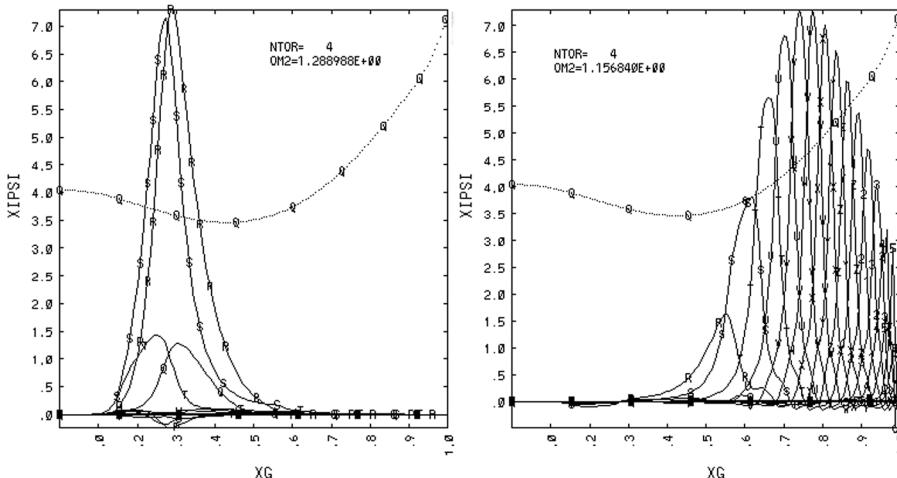


FIG. 7. The structure of modes localized around $r = 0.25$ and $r = 0.75$ for shot # 142111 at $t = 675$ ms as computed by NOVA for $n = 4$. The dotted line is the safety factor profile.

marginally stable AEs. Following the procedure described in Sec. III B for calculating the functional form of the rates, we first use Eq. (25) to compute the growth rates and Eqs. (18)–(21) for the damping rates. We then use the results from NOVA-K simulations as given in Sec. V A to calibrate the analytical growth rate profiles using the two-point normalization scheme described in Sec. III D. Fig. 8 depicts the 1.5D computed relaxed profiles. For $t < 600$ ms, we run NOVA-K for the two cases separately to calibrate the analytic expressions; however, for the two cases where $t > 600$ whose safety factors measurements are not optimized, we use the normalization rates calculated for $t = 360$ ms to compute the resulting distribution function and compare it to FIDA results. To avoid redundancy, we only present the resulting profile redistribution for $t = 360$ ms as a representative of the times $t < 600$ ms where losses occur. The 1.5D predicted losses for these cases are provided in Fig. 9. We report that the simulated losses and flattening for $t = 410$ ms are similar to $t = 360$ ms. The 43% neutron losses for $t = 410$ ms further supports the results of the represented $t = 360$ ms case.

We compare the predicted neutron losses from the 1.5D model and the experimentally measured neutron deficit for DIII-D discharge # 122117. The ratio of the neutron emission rate to the classical rate is computed using Eq. (24) and is represented in Fig. 9 as crosses in juxtaposition with the experimentally measured values. The predicted emission rates are quite close to the measured neutron loss rate.

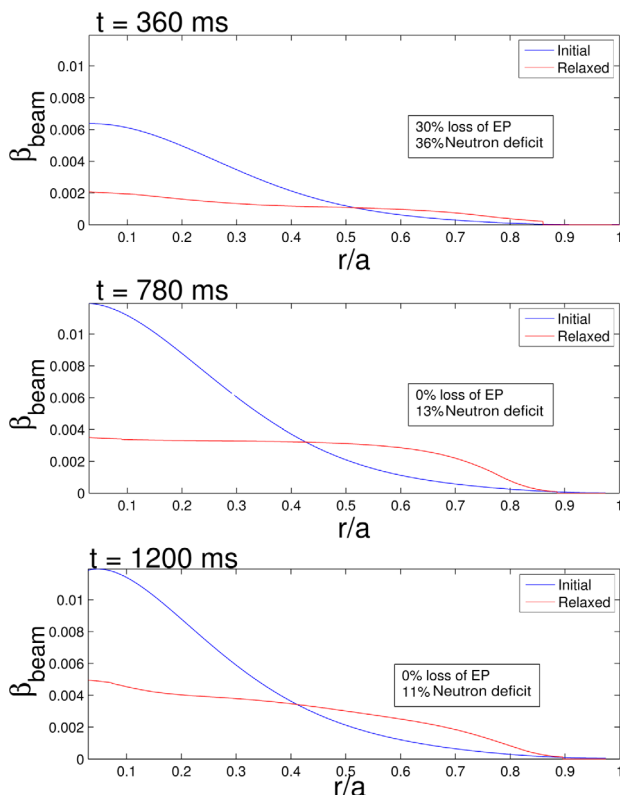


FIG. 8. Redistribution of energetic particles at $t = 360$ ms results in significant EP losses and associated neutron losses. At later times, AE activity results in the redistribution of particles without EP losses.

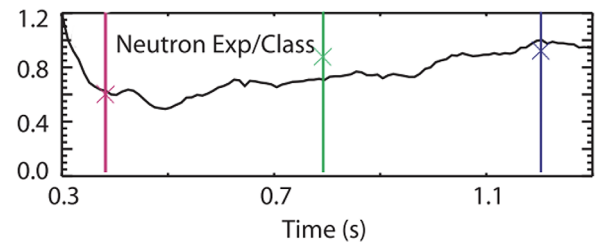


FIG. 9. The time evolution of the ratio of the measured neutron emission to TRANSP computed classical rate is represented by a solid line. Juxtaposing the experimental results, the emission rates calculated by the 1.5D model are represented with colored crosses at the times of interest, $t = 360$ ms (red), 780 ms (green), and 1200 ms (blue). Reprinted with permission from W. W. Heidbrink *et al.*, Nucl. Fusion **48**, 084001 (2008). Copyright 2008 IOP Publishing Ltd.

2. Discharge #142111

As discussed in Sec. IV B, there are measurements of AE induced EP losses that peak around $t = 525$ ms. Although AE activity persists throughout most of the shot, the associated losses diminish after $t = 800$ ms.

In this section, we present the results of 1.5D applied on # 142111 depicting this qualitative change and making estimates of the expected losses. As shown in Fig. 10, AE activity around $t = 425$ ms causes redistribution of energetic particles contained within the last closed flux surface without resulting in losses. Modification of the EP pressure profile, however, results in some neutron losses in accordance with Eq. (24). TAE activity increases at $t = 525$ ms and EP redistribution now extends all the way to the last closed flux surface resulting in their loss.

As time evolves, losses continue to occur up to $t \approx 800$ ms where the system reverts to transport and redistribution of EP without any losses. This is depicted in Fig. 10 for $t = 925$ ms where the particles are redistributed due to the unstable central modes but the redistribution is contained within the last closed flux surface.

We use results reported by Van Zeeland¹⁹ on the experimental measurements of the neutron emission rate in comparison to the TRANSP expectations to validate the predictions of 1.5D. In Fig. 11, we present the model's results in juxtaposition with the measurements of Van Zeeland.

C. Discussion

We report good agreement of the 1.5D model with experimental measurements of DIII-D discharges #122117 and #142111. We elaborate here on some remarks regarding the 1.5D results reported.

AE activity does not need to be associated with losses of energetic particles. This is an important feature that 1.5D captures by modeling the quasilinear diffusion of particles as described in Sec. III B. The basic idea is that particles undergo diffusion and are redistributed in phase space such that the pressure gradient is maintained below the critical value that destabilizes the modes.

The critical value of the gradient in EP pressure is proportional to the ratio of the damping to the growth rate of TAE modes. Therefore, when the ratio is high, particles can

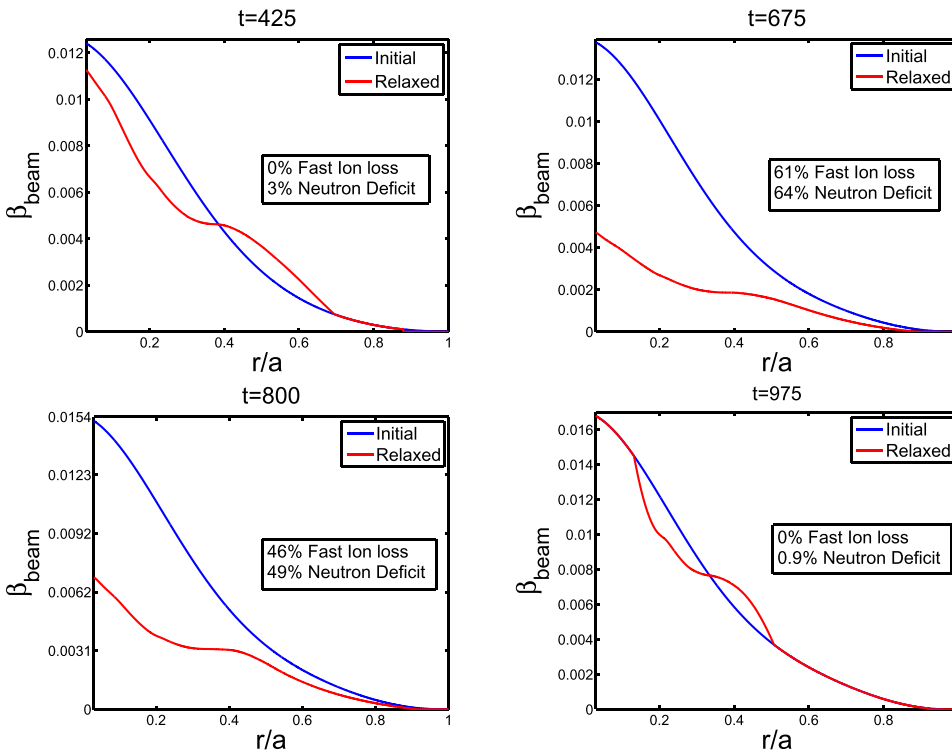


FIG. 10. Relaxation of EP distribution for different time slots. EP losses peak at around $t=525$ ms, while AE activity is evident throughout. At $t=425$ ms and at $t=975$ ms, TAE activity only results in redistribution of EP without resulting losses.

stack up and maintain a steep gradient without destabilizing the modes, i.e., when there is significant damping, the free energy from the gradient in EP pressure profiles is not enough to destabilize the modes. However, if this ratio is low the free energy can be strong enough to destabilize the mode. The associated low critical gradient models a high quasilinear diffusion coefficient which continues to redistribute the particles until the gradient reduces to or below the critical value at which the mode is stable.

In cases where the critical gradient in EP pressure is lower than the original gradient around the center but significantly higher at the edge, energetic particles undergo diffusion that will transport them from the center towards the edge. However, due to the high critical gradient threshold at the edge, particles can accumulate without being transported beyond the last closed flux surface. This results in redistribution and central flattening without any losses to the wall as AE modes saturate.

On the other hand, in cases where the critical value of the gradient is not sufficiently high towards the edge, diffusion results in particles being transported beyond the last closed surface and consequently results in particle losses.

We also note the discrepancy in the neutron loss measured to that predicted by the 1.5D model for $t \approx 975$ and $t \approx 425$ in discharge # 142111. There are other modes prevalent in these cases whose effects are not captured by the model. Most notably, the EGAM might cause neutron deficit at 425 ms, while BAAEs result in EP transport and neutron deficit at 925 ms. EGAMs are symmetric modes ($n=0$) which result in EP transport in velocity space only. However, this affects the cross section for neutron emission rates, which could lead to neutron deficit. The discrepancy might have been caused by a deficiency in input to TRANSP and thus NOVA. Therefore, the stability calculations performed by NOVA-K may be questionable especially some damping rates that are very sensitive to plasma profiles such as the continuum damping. Overall these discrepancies reflect a deficiency of the stability calculation.

Due to the sensitivity of the 1.5D model results on NOVA-K calculations used for normalization, discrepancy arises if certain growth and/or damping mechanisms are excluded.

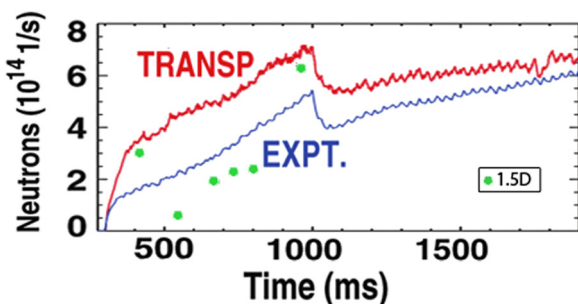


FIG. 11. TRANSP predicted (red) and experimentally measured (blue) neutron emission rate as a function of time. We add to the figure green dots as markers for the 1.5D results for neutron rates at $t=425$, 525, 675, 725, 800, and 975 ms. Adapted from Ref. 19. Adapted from M. A. Van Zeeland, Phys. Plasmas **18**, 056114 (2011). Copyright 2011 American Institute of Physics.

VI. SUMMARY AND FUTURE WORK

In this work, we have combined the established routines, NOVA and NOVA-K with the newly developed 1.5D. The code NOVA calculates the eigenmode structure while NOVA-K determines the contributions of growth and damping rates. NOVA is used to find two eigenmodes, one tending to be localized in the center of the plasma and the other towards the edge. The new code 1.5D uses the NOVA-K

computed rates for these two eigenmodes to normalize the rates that are analytically computed for all radial positions.

Then, in 1.5D, we presume that the profiles relax to a locally marginal state at every radial position where the local drive exceeds the local damping. With the constraint that the energetic particle number be conserved during the profile relaxation, providing the redistribution region does not reach the loss region, the change of profile can then be computed. If the instability region reaches the plasma edge, then the constraint on the conservation of particles is released and the profile is integrated using the critical value of the gradient for which the mode is marginally stable. This results in a profile where $(\int dr \beta_{ini}(r) - \int dr \beta_{rlx}(r)) / \int dr \beta_{ini}(r) > 0$ is the fraction of EP loss.

The well diagnosed DIII-D discharges # 142111 and #122117 have shown significant TAE activity and correlated neutral beam losses and profile redistributions. We use these discharges to validate the proposed 1.5D model. The model predicted losses that agree with the experimentally measured ones, and the relaxed profiles computed by 1.5D depicts the flattening measured by FIDA.

The strength of the model is in predicting the relaxed profiles in an efficient and quick way without detailed computations of the fields and wave-particle interactions. 1.5D model can be used as an initial check for EP losses in a large parameter space. This then can be followed by more detailed simulations in a specific parametric subspace of interest.

A. Application to ITER

The model is being developed for the purpose of predicting the effect of AE modes on energetic particles in ITER and other burning plasmas where alpha confinement is crucial. The success of the model in predicting the redistribution of EP in DIII-D and making ballpark estimates of the neutron losses gives us confidence in applying it to ITER. The model is yet to be expanded to include two species, isotropic and anisotropic particle distribution functions, which is necessary for ITER applications, especially when an additional energetic particle source from neutral beam injection is present.

B. Line broadening quasilinear burst model

This work is a promising initial investigation of a quasilinear treatment of energetic particle interaction with Alfvénic Eigenmodes. The resulting agreement with experimental measurements motivates a more sophisticated model, LBQ3D, currently being developed. LBQ3D is a fully dimensional

extension to toroidal geometry of the proposed Line Broadened Quasilinear model,¹⁴ LBQ, which has been implemented on the one dimensional bump on tail problem.

ACKNOWLEDGMENTS

This work has been supported under DOE Contract No. DE-AC02-09CH11466.

- ¹H. L. Berk and R. Mett, *Phys. Fluids B* **5**, 3969 (1993).
- ²H. L. Berk, J. VanDam, J. Candy *et al.*, *Phys. Plasmas* **2**, 3401 (1995).
- ³H. L. Berk, B. Breizman, and H. Ye, *Phys. Lett. A* **162**(2), 475–481 (1992).
- ⁴H. L. Berk, B. Breizman, and H. Ye, *Phys. Rev. Lett.* **68**(24), 3563 (1992).
- ⁵R. Betti and J. P. Freidberg, *Phys. Fluids B* **4**, 1465 (1992).
- ⁶R. V. Budny, *Nucl. Fusion* **42**, 1383 (2002).
- ⁷J. Candy, *Plasma Phys. Controlled Fusion* **38**, 795 (1996).
- ⁸J. Candy and M. N. Rosenbluth, *Nucl. Fusion* **35**, 1069 (1995).
- ⁹C. Z. Cheng, *Phys. Rep.* **211**, 1–51 (1992).
- ¹⁰H. H. Doung, W. W. Heidbrink *et al.*, *Nucl. Fusion* **33**, 749 (1993).
- ¹¹W. Drummond, C. Pines *et al.*, in *Proceedings of the International Conference on Plasma Physics and Controlled Thermonuclear Fusion* (Salzburg, 1961), p. 134.
- ¹²A. Fasoli *et al.*, *Nucl. Fusion* **47**(6), S264 (2007).
- ¹³D. Borba *et al.*, “The influence of plasma shaping on the damping of toroidal Alfvén eigenmodes,” in 23rd IAEA Fusion Energy Conference, Daejeon, Korea, 2010.
- ¹⁴H. L. Berk *et al.*, *Nucl. Fusion* **35**, 1661 (1995).
- ¹⁵H. L. Berk *et al.*, *Phys. Fluids B* **4**(7), 1806 (1992).
- ¹⁶K. L. Wong *et al.*, *Phys. Rev. Lett.* **76**, 2286 (1996).
- ¹⁷K. L. Wong *et al.*, *Plasma Phys. Controlled Fusion* **41**, R1–R56 (1999).
- ¹⁸M. A. Van Zeeland *et al.*, *Phys. Rev. Lett.* **97**, 135001 (2006).
- ¹⁹M. A. Van Zeeland *et al.*, *Phys. Plasmas* **18**, 056114 (2011).
- ²⁰M. Saigusa *et al.*, *Plasma Phys. Controlled Fusion* **40**, 1647 (1998).
- ²¹N. N. Gorelenkov *et al.*, *Nucl. Fusion* **43**, 594 (2003).
- ²²N. N. Gorelenkov *et al.*, *Phys. Rev. Lett.* **95**, 265003 (2005).
- ²³R. K. Fisher *et al.*, *Rev. Sci. Instrum.* **81**, 10D307 (2010).
- ²⁴R. White *et al.*, *Plasma Phys. Controlled Fusion* **52**, 045012 (2010).
- ²⁵S. E. Sharapov *et al.*, *Nucl. Fusion* **45**, 1168–1177 (2005).
- ²⁶W. W. Heidbrink *et al.*, *Phys. Fluids B* **5**(7), 2176 (1993).
- ²⁷W. W. Heidbrink *et al.*, *Phys. Rev. Lett.* **71**, 855 (1993).
- ²⁸W. W. Heidbrink *et al.*, *Phys. Rev. Lett.* **99**, 245002 (2007).
- ²⁹W. W. Heidbrink *et al.*, *Nucl. Fusion* **48**, 084001 (2008).
- ³⁰W. W. Heidbrink *et al.*, *Phys. Plasmas* **15**(5), 055501 (2008).
- ³¹G. Y. Fu and J. W. Van Dam, *Phys. Fluids B* **1**(10), 1949–1952 (1989).
- ³²G. Y. Fu, H. L. Berk, and A. Pletzer, *Phys. Plasmas* **12**, 082505 (2005).
- ³³T. Fulop, *Plasma Phys. Controlled Fusion* **38**, 811 (1996).
- ³⁴N. N. Gorelenkov and S. E. Sharapov, *Phys. Scr.* **45**, 163–166 (1992).
- ³⁵O. D. Gurcan, P. H. Diamond, and T. S. Hahm, *Phys. Plasmas* **13**, 052306 (2006).
- ³⁶A. N. Kaufman, “Quasilinear diffusion of an axisymmetric toroidal plasma,” *Phys. Fluids* **15**, 1063 (1972).
- ³⁷Y. Kolesnichenko, *Nucl. Fusion* **20**, 727 (1980).
- ³⁸G. Y. Fu *et al.*, *Phys. Fluids B* **4**, 3722 (1992).
- ³⁹R. Mett and S. Mahajan, *Phys. Fluids B* **4**, 2885 (1992).
- ⁴⁰S. Bernabei *et al.*, *Phys. Plasmas* **6**(5), 1880 (1999).
- ⁴¹A. A. Vedenov, *J. Nucl. Energy, Part C* **5**, 169–186 (1963).